Modelling of Hull Roughness

MODELLING OF HULL ROUGHNESS

N. Speranza, School of Engineering, Institute for Energy Systems, University of Edinburgh, UK
B. Kidd, AkzoNobel, UK, barry.kidd@akzonobel.com
M. P. Schultz, Department of Naval Architecture & Ocean Engineering, United States Naval Academy, USA, mschultz@usna.edu
I. M. Viola*, School of Engineering, Institute for Energy Systems, University of Edinburgh, UK, i.m.viola@ed.ac.uk
** Corresponding author*

Abstract

In this paper we present a practical guideline on how to estimate the frictional resistance of ship hulls due to different fouling control coatings. Most of the current methods rely on empirical formulations based on an equivalent sand grain roughness height. These correlations are not universal and cannot be applied to every marine surface. Conversely, the shear stress of a specific coating can be measured in an experimental facility at the same Reynolds roughness number as at full scale. The results can be used to inform the boundary conditions of computational fluid dynamics, where the complex flow around the ship can be computed for any sailing condition. Hence, this methodology allows the estimation of the frictional resistance due to a specific surface in a specific sailing condition. Representative antifouling coating products by AkzoNobel, and wall functions for the open-source code OpenFOAM, are used to illustrate the methodology. Similarities and differences with other methods are discussed.

1 INTRODUCTION

The effect of roughness on the frictional resistance of marine vessels increases with the cruising speed. However, the frictional contribution to the total resistance depends mostly on the Froude number, thus low or moderate speeds are expected to be the most influenced by hull roughness. These conditions are especially met by low-speed, large ships. Conversely, the relative increase of resistance due to the roughness is less significant for powerboats and superyachts, because for these vessels the wave resistance is considerably more significant than the frictional resistance. At least for some sailing conditions, roughness effects would be significant for sailing crafts, which span a wide range of velocities during navigation. Moreover, on small and slow crafts such a small cruising boat, a significant part of the boundary layer of the hull and appendages is laminar. Therefore, frictional resistance can significantly increase because roughness promotes laminar-to-turbulent transition of the boundary layer. Braslow and Knox [1], for instance, have developed a methodology to calculate the critical roughness height that would cause transition. However this effect is not considered in the present paper, which deals with the frictional resistance in a fully turbulent boundary layer.

Most of the experimental evidence on the impact of fouling [2], marine coatings roughness [3, 4] and hull irregularities [5, 6] on frictional resistance has been conducted for ship hulls. However, most of these results can be applied to any immersed body. The resistance of scaled models can be measured with towing tank tests [7, 8, 9]. Using the approach of Hughes [10], the measured resistance is broken down into wave resistance and frictional resistance. The wave resistance scales with the Froude number, while the frictional resistance scales with the Reynolds number. Therefore model scale experiments are performed at the same Froude number as full scale, and then the frictional resistance is scaled to the full scale Reynolds conditions. The added frictional resistance ΔR due to roughness can be taken into account adding the allowance correlation proposed by Townsin [11],

$$\Delta R = \left\{ 44 \left[\left(\frac{k_s}{L} \right)^{1/3} - 10 Re^{-1/3} \right] + 0.125 \right\} \times 10^{-3}, \tag{1}$$

where L is the length of the hull and k_s is the equivalent sand grain roughness height, here taken as the Mean Apparent Amplitude of the roughness as measured by a BSRA Hull Roughness Analyser. It is important to note that the equivalent sand grain roughness height is, in this case, taken as a geometric property of the surface. No general agreement exists on the validity of the above formula, as other experimental studies have suggested that frictional resistance of a rough marine surface could not be described by solely using a measure of its height. In fact, the frictional resistance could also depends on the roughness texture, slope and form [4, 12, 13].

Computational Fluid Dynamics (CFD) simulations offer a viable alternative to towing tank tests [14]. In particular, Reynolds-Averaged Navier-Stokes (RANS) simulations are now being used extensively for various design problems in the industry; a review is given in Viola *et al.* [15]. Recommended procedures for ship CFD applications are given by the ITTC [16]. An example of CFD simulations for the design of America's Cup yacht hulls is given in Viola *et al.* [17]. When wall roughness effects are added in RANS computations (*e.g.* [18, 19, 20, 21]), no approach is shown to be able to handle the variety of roughness topologies encountered in the marine sector. Most of the approaches are based on the equivalent sand grain roughness height k_s (*e.g.* [18, 19]), which is presented in detail in the next section. The geometry of the rough surface is often characterised by one geometric property, and the frictional resistance is scaled with the Reynolds number based on this dimension. Unfortunately, this is not sufficient to characterise the rough geometry and to enable the prediction of its effect on the frictional resistance over a wide Reynolds number range [22].

It is not know how the frictional resistance depends on the specific surface topology. For this reason a methodology that does not rely on geometric measurements of the rough surface is here proposed. Every surface must be treated separately and its frictional properties tested experimentally [22]. This approach was followed by Leer-Andersen and Larsson [23], who suggested an experimental-numerical procedure to include experimental results into a commercial boundary-element software. Following this approach, in the present paper the experimental data are fed to *ad hoc* wall-functions for a RANS code.

The proposed methodology starts from the estimate of the flow conditions at which the frictional properties of the marine surface should be measured. Different approaches are presented and compared using realistic values of antifouling coatings. We consider two case studies: a small hull of length 3.048 m sailing at 3.9 knots and a 220-m-long hull sailing at 14.5 knots. We will show that while the flow conditions on the hull varies significantly from the bow to the stern, only a limited range of these conditions can be considered for the experimental measurements. A sample of the marine surface should be tested at these conditions and experimental friction data should be fitted into a newly proposed correlation function, which is implemented in a wall function for RANS simulations. In particular, here the formulation of a wall function sensitised to the pressure gradient is presented for a $K-\epsilon$ turbulence model in the open-source CFD code OpenFOAM.

The rest of the paper is organised as follows. Firstly, some theoretical considerations on turbulent boundary layers over rough walls are presented (Sec. 2), followed by a description of the overall methodology (Sec. 3). Different approaches for the estimate of flow conditions are shown in Sec. 3.2, and experimental methods for measuring frictional properties of rough surfaces are reviewed in Sec. 3.3.2. The proposed fitting of the experimental data is presented in Sec. 3.4, followed by the formulation of the wall function in Sec. 3.5. In Sec. 4, the two case studies are considered. Finally, the main conclusions of the paper are summarised in Sec. 5.

2 THEORETICAL CONSIDERATIONS

Predicting the flow over rough surfaces has been the objective of several studies for over a century. Excellent reviews are given, for instance, by Raupach *et al.* [24] and by Jimenez [25]. In the following, only the relevant quantities needed to describe the methodology are introduced.

There are many different ways to characterise a rough surface. In the following we adopt the average roughness height R_a as defined by Shultz [26]. This is measured over a 50 mm length of the coated surface, as

$$R_a = \frac{1}{n}\sum_{i=1}^{n}|y_i|, \tag{2}$$

where y_i is the normal distance from the centreline of the rough surface.

The flow around a hull is a function of two geometrical scales, the ratio between the boundary layer thickness δ and the viscous length δ_ν, and the ratio between the roughness size (*e.g.* R_a) and δ_ν. The first scale is set by the friction Reynolds number $Re_\tau = \delta/\delta_\nu$, which grows from 0 at the bow (where $\delta = 0$) to ca. 10^4 at the stern. The second scale is the roughness Reynolds number (*e.g.* R_a/δ_ν), is infinite at the bow and decreases approaching the stern.

The fully-developed flow in a channel with a constant pressure gradient is a convenient paradigm of the flow over a hull. In fact, the boundary layer flow is significantly more challenging to achieve, both experimentally and numerically, than a fully-developed channel flow. For the latter, the maximum Re_τ that can be achieved in a laboratory, or with equally-accurate direct numerical simulations, is of the order of 10^3. Therefore the flow conditions at the stern of the hull cannot be replicated and the skin friction of the hull at full scale must be extrapolated from lower Re_τ experiments. Conversely, the roughness Reynolds number (*e.g.* R_a/δ_ν), can be matched experimentally in a fully-developed channel flow facility.

If the wall is smooth, there is a distance y from the wall where the flow velocity u depends *only* on the wall shear stress τ_w. Therefore we define a non-dimensional velocity u^+ and a wall distance y^+ based on τ_w:

$$u^+ \equiv \frac{u}{u_\tau}, \tag{3}$$

$$y^+ \equiv \frac{y}{\delta_\nu}, \tag{4}$$

where

$$u_\tau \equiv \sqrt{\frac{\tau_w}{\rho}}, \tag{5}$$

$$\delta_\nu \equiv \frac{\nu}{u_\tau}. \tag{6}$$

The velocity is uniquely defined by the overlap logarithmic law of the wall,

$$u^+ = \frac{1}{\kappa}\ln y^+ + B, \tag{7}$$

where $\kappa \approx 0.41$ is the Von Karman constant, $B \approx 5.1$, and ν, ρ are the kinematic viscosity and density of the fluid, respectively. Given u and y, Eq. 7 can be solved iteratively to find τ_w.

In *fully rough* conditions, when the size of the roughness is large compare to the viscous length (*e.g.* $R_a/\delta_\nu \gg 1$), the velocity u^+ depends on the equivalent sand grain roughness height k_s, and not on τ_w. Equivalently, the frictional resistance coefficient depends only on the roughness Reynolds number (R_a/δ_ν) and not on the friction Reynolds number (Re_τ). Nikuradse [27] found that, in these conditions, the overlap logarithmic law of the wall can be expressed as

$$u^+ = \frac{1}{\kappa} \ln \frac{y}{k_s} + 8.5. \tag{8}$$

Given u^+ and y, the equivalent sand grain roughness height k_s can be computed from Eq. 8. Therefore k_s is a hydrodynamic length scale and thus a property of the flow that does not depend explicitly by any geometric parameter of the roughness. The name of this hydrodynamic length scale is due to the fact that Nikuradse [27], who pioneered this research area, used sand grains of various diameters to change the roughness of pipes, and k_s was the average diameter of the grains. Successively, the measured hydrodynamic length scales of different rough surfaces have been correlated with the k_s used by Nikuradse. For example, Schlichting [28] tested a wide range of rough surfaces in fully rough conditions and, for each of these, found the equivalent sand grain roughness height k_s that provided the measured drag when used with Nikuradse's correlations.

The overlap logarithmic law of the wall can be written isolating the velocity difference ΔU^+ between the smooth and the rough condition, hence

$$u^+ = \frac{1}{\kappa} \ln y^+ + 5.1 - \Delta U^+. \tag{9}$$

ΔU^+, also called roughness function, is used to describe the observed downward shift of velocity respect to the smooth case [29]. In fully rough conditions, ΔU^+ can be computed subtracting Eq. 7 to Eq. 8, resulting in

$$\Delta U^+ = \frac{1}{\kappa} \ln k_s^+ - 3.4, \tag{10}$$

where

$$k_s^+ \equiv \frac{k_s}{\delta_\nu}. \tag{11}$$

An elegant proof that, in the limiting condition where $R_a/\delta_\nu \to \infty$, the drag coefficient at a fixed point on the hull is constant with the ship speed, is given by Pullin *et al.* [30]. Similarly, at a fixed point on the hull, also the boundary layer thickness is constant with the ship speed. Conversely, for an hypothetically smooth hull, the boundary layer thickness would decrease with the ship speed. Pullin and co-authors derive these results from a logarithmic velocity profile (Eq. 9), also including the wake function, which we have neglected.

In *transitionally rough* conditions, when R_a/δ_ν is not sufficiently high to achieve fully rough conditions, the velocity u^+ depends on both τ_w and k_s, therefore ΔU^+ is unknown. The flow over a hull can range from fully rough in the first few meters from the bow to transitionally rough on the rest of the hull.

Colebrook [31] provided an equation to compute the Darcy friction factor as a function of k_s and the Reynolds number based on the pipe's diameter. Jimenez [25] showed that this equation can be written in an explicit form for the roughness function as

$$\Delta U^+ = \frac{1}{\kappa} \ln \left(1 + 0.26 k_s^+\right). \tag{12}$$

In this formulation, k_s must be determined in fully rough conditions. When the fluid is water and the roughness height is as small as that of typical marine coatings, the fully rough regime cannot be easily achieved because of limitation in the maximum velocity that can be typically achieved in a laboratory. Hence, k_s cannot be measured for marine surfaces.

Previous authors [3, 12, 13, 32, 33, 34, 35, 36, 37] have suggested a range of correlations between the geometric features of the rough surface and k_s. For instance, through experiments on antifouling coatings, Schultz [3] found a good correlation between the measured roughness function and that computed with $\Delta U^+ = \frac{1}{\kappa} \ln (1 + k_s^+)$, where $k_s = 0.17 R_a$. This is equivalent to using

$$k_s = 0.61 R_a \tag{13}$$

with Eq. 12. However, no universal correlation is shown to work for the variety of marine surfaces existing in nature. Thus, it is believed that every specific surface should be tested experimentally and the frictional characteristic ΔU^+ should be measured.

3 PROPOSED METHODOLOGY

3.1 OVERVIEW

The proposed methodology foresees that experimental measurements are performed for each surface that has to be considered. For example, to estimate the difference in the frictional resistance of a ship when coated with two different antifouling coatings, sample of both of these two coatings have to be tested in a laboratory. The results of these measurements are then used as input for CFD simulations, where the full-scale ship can be modelled in different sailing conditions. Hence, this methodology does not require full scale measurements, but relatively simple integral measurements in a small-scale facility.

The roughness of a surface depends on the material, on the manufacture process, the finishing, *e.t.c.*. Therefore, it is not possible to produce a model-scale sample of a rough surface. While the hull geometry can be scaled, R_a cannot be scaled. In order to highlight this important concept, a dimensional notation is used for R_a and the other associated fluid mechanics quantities that cannot be scaled. Since R_a cannot be scaled, a methodology must be proposed that foresees testing a sample of the full-scale rough surface in a laboratory at the same roughness Reynolds number experienced at full-scale. Likely, over a portion of the hull that accounts for at least 99% of the frictional resistance, the ratio R_a/δ_ν has values that can be easily achieved in a fully-developed channel flow facility. Therefore, for the range of flow conditions that matters, ΔU^+ can be measured in a laboratory at the same δ_ν and τ_w than at full scale. This will be demonstrated in the Sec. 3.3.1.

While δ_ν varies continuously along the hull's boundary layer, δ_ν is constant over the length of the channel. Therefore, for each velocity tested in a fully-developed channel flow facility, the measured ΔU^+ corresponds to that of a full-scale the boundary layer at one specific distance from the bow.

3.2 ESTIMATE OF THE FULL-SCALE FLOW CONDITIONS

This section shows how to estimate analytically the range of δ_ν that should be tested experimentally. Consider a hull long L sailing at a speed U, and a coordinate x from the bow, positive towards the stern. Very near to the bow, δ_ν is very small and it cannot be replicated in a laboratory. This will be further discussed in Sec. 3.3.1. In order to achieve an accurate roughness for all the ship hull, experiments should be performed for a range of δ_ν: from the smallest possible achievable in the facility to the maximum δ_ν at the stern ($x = L$). Here we present a criteria to estimate the minimum δ_ν that should be tested in the facility.

It is proposed not to consider the small values of δ_ν in the region near the bow that contributes to less than 1% to the total frictional resistance. If the small values of δ_ν in this region are not matched experimentally, and the roughness function is extrapolated from tests performed at higher values of δ_ν, the error on the total frictional resistance can be expected to be smaller than 1% (assuming that matching the exact friction Reynolds number is sufficient to achieve the exact frictional resistance). In fact, in this way, the effect of the roughness is exactly replicated for all the ship length but for a small region near the bow, which account for less than 1% of the total frictional resistance. In this region, the effect of roughness is not neglected, but it is extrapolated from the experiments performed at larger δ_ν.

The distance x_0 that delimits the part of hull that accounts for 1% of the total frictional resistance can be computed as follow. The frictional resistance R_{x_0} due to the part of the hull between x_0 and the stern ($x = L$) is

$$R_{x_0} = \int_{x_0}^{L} \frac{1}{2} \rho c_f b \mathrm{d}x, \tag{14}$$

where ρ is the water density, $b = b(x)$ is the wetted length of the hull station at the coordinate x, and

$$c_f = 2 \left(\frac{\nu}{\delta_\nu U} \right)^2. \tag{15}$$

If the distribution of $c_f = c_f(x)$ is known, then Eq. 14 can be used to find the lower limit of integration x_0 such that R_{x_0} is 99% of the total frictional resistance R_L (which is computed using Eq. 14 with limits of integration 0 and L). Three different approaches are presented here, from a simple analytical method, to the most accurate numerical method that accounts for the effect of the roughness. These approaches consider the flow over a flat plate with a zero thickness, *i.e.* without a stagnation point at the leading edge. The hull, however, has a stagnation point at the bow, and thus the frictional resistance is locally different from that of a flat plate.

3.2.1 POWER LAW APPROACH

The friction coefficient can be found using different formulations, as a function of the local Reynolds number $Re = xL\nu^{-1}$. The simplest approach is to assume a universal velocity profile described by, for instance, the $1/7^{th}$ power law. This assumption results in [38]:

$$c_f = \frac{0.027}{Re^{1/7}}. \tag{16}$$

If a constant hull width b is assumed, then the integral in Eq. 14 can be solved analytically and the condition $R_{x_0}/R_0 = 99\%$ gives $x_0 \approx 0.5\%L$. The lower and upper values of δ_ν that should be investigated in the fully-developed channel flow facility are found substituting L and x_0, respectively, in Eq. 16, and evaluating Eq. 15 for the two results.

3.2.2 SCHOENHERR'S APPROACH

Another empirical approach based on force measurements on flat plates, is the formula proposed by Schoenherr [39]. For each x in range $[0, L]$ the mean skin friction coefficient ($C_F = R_L/(1/2\rho U^2 S)$, where S is the wetted surface) of a flat plate can be found solving iteratively Eq. 17:

$$\frac{0.242}{\sqrt{C_F}} = \log ReC_F. \tag{17}$$

Less known than Eq. 17, is the equation for the local skin friction c_f that was derived by Schoenherr differentiating Eq. 17. For each C_F the local skin friction c_f at the distance x from the bow is

$$c_f = \frac{0.558 C_F}{0.558 + 2\sqrt{C_F}}. \tag{18}$$

3.2.3 GRANVILLE'S APPROACH

The more general formulation proposed by Granville [40] can be used to account for the effect of roughness and of the wake function on the resistance of the flat plate. Granville derived a correlation between the streamwise coordinate x and the viscous length scale δ_ν:

$$x = \left[\delta_\nu Re_\theta\right]_x - \frac{2U_b}{\nu} \int_0^{\left[\delta_\nu\right]_x} Re_\theta \delta_\nu d\delta_\nu, \tag{19}$$

where

$$Re_\theta = \left(I_1 - I_2 \frac{\nu}{U_b \delta_\nu} \right) e^{\kappa \left(\frac{U_b \delta_\nu}{\nu} - 5.1 + \Delta U^+ - \frac{2\Pi}{\kappa} \right)}, \tag{20}$$

$$I_1 \equiv \frac{11}{12\kappa} + \frac{\Pi}{\kappa}, \tag{21}$$

$$I_2 \equiv \frac{4819}{2520} \frac{1}{\kappa^2} + \frac{639}{420} \frac{2\Pi}{\kappa^2} + \frac{13}{35} \frac{4\Pi^2}{\kappa^2}. \tag{22}$$

The operator $[A]_x$ requires that the argument A is evaluated at the coordinate x from the bow, Π is the Coles' wake intensity parameter that can be measured experimentally. A reference value of 0.55 can be used for boundary layers with zero pressure gradient [41].

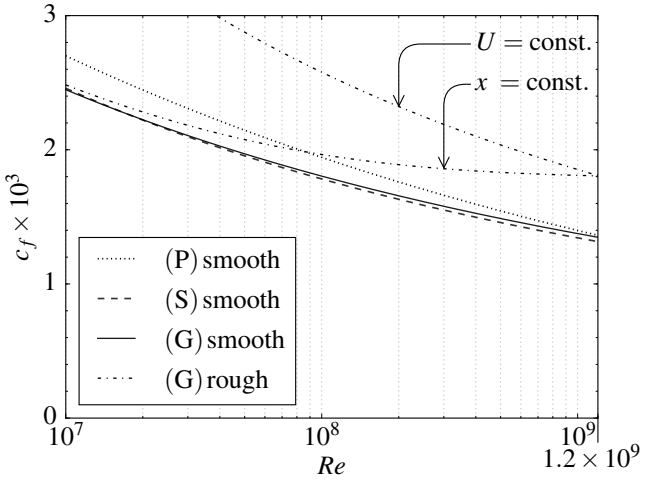

Figure 1: Difference in skin friction coefficient distribution over Re between the friction lines (P) based on $1/7^{th}$ power law, (S) based on Schoenherr [39] and (G) based on Granville [40] for smooth and two rough cases: x-varying at fixed $U = 14.5$ knots and U-varying at fixed $x = 220$ m (ΔU^+ from Eqs.12-13 with $R_a = 400$ μm).

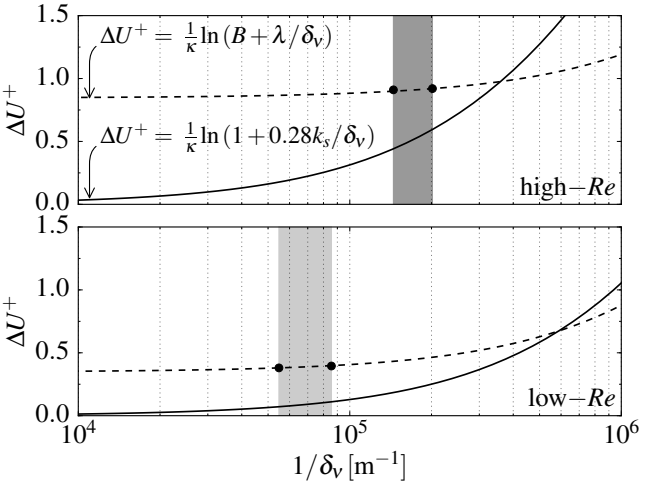

Figure 2: Coloured bars: intervals of $1/\delta_\nu$ to compute 99% of the total skin frictional resistance of a 3.048-m-long flat plate at 3.9 knots (bottom) and a 220-m-long flat plate at 14.5 knots (top). Granville's approach with ΔU^+ from Eqs. 12-13 (solid lines) is used for the computation with $R_a = 3.2$ μm (bottom) and $R_a = 8.1$ μm (top). Solid circles are samples of experimental data for the two rough surfaces. Dashed lines show the fitting of Eq. 25 with $A = 1/\kappa$ (bottom: $B = 1.15$, $\lambda = 0.28$ μm; top: $B = 1.41$, $\lambda = 0.21$ μm).

Using, in first approximation, the experimental relation of Colebrook [31] in Eq. 12 with Eq. 13, ΔU^+ can be expressed as a function of δ_ν and substituted into Eq. 20. For a hull velocity U and a given surface roughness R_a, Eq. 19 can be solved iteratively to find δ_ν for each x. The iterative procedure consists in guessing a value of $[\delta_\nu]_{x^*}$; evaluate numerically the integral in Eq. 19; and compute the real value of x corresponding to the guessed $[\delta_\nu]_{x^*}$. When the viscous length corresponding to $x = L$ is found, the procedure is repeated for a lower value of $[\delta_\nu]_{x^*}$, thus spanning backward all the lengths from L to 0.

3.2.4 COMPARISON OF THE METHODS

Figure 1 shows a comparison between the friction lines of the power law (P), Schoenherr (S) and Granville (G) for a smooth surface. The friction coefficient plotted here is the local c_f at the coordinate $x = Re\,\nu U^{-1}$ along the hull. The Coles' wake intensity is set to $\Pi = 0.55$. The friction lines (G) and (S) show good agreement for $Re \in [10^7, 10^8]$, which covers most of the hull's surface of sailing crafts, but just a fraction of modern ships' hulls. Namely, taking 14.5 knots as a reference speed and $\nu = 1.35 \times 10^{-6}$ m^{2}s^{-1}, this range of Re corresponds to a distance from the bow $x \in [1.8, 18]$ m. The friction line obtained with (P) significantly over-predicts c_f, but the difference decreases with Re. Yet, at $Re = 10^8$, the c_f predicted with (P) is more than 7% higher than the ones computed with (S) and (G).

For instance, taking $R_a = 400$ μm (cf. dash-dotted lines in Fig. 1) as representative of a marine surface fouled for one year, an increase of 33% is computed respect to the smooth friction lines at $Re = 1.2 \times 10^9$. This difference is even higher at lower Re when x is varied, *i.e.* following the curve $U = $ const. in Fig. 1. However, when $R_a \lessapprox 10$ μm (not shown in Fig. 1), which is a condition typically satisfied by newly coated surfaces, the effect of the roughness computed with the method of Granville is small. In the scale of Figure 1, a curve computed with the method of Granville for $R_a = 10$ μm would almost overlap with the curve computed with the same method for a smooth surface. The difference between a smooth surface and a newly cocated surface, in fact, is smaller that the differences between the values predicted by the different methods for smooth surfaces. Therefore, for smooth and moderate roughness, it is not worth using the more complicated method of Granville. Conversely, this method can be considered for very rough surfaces and, particularly, at low Re.

3.2.5 EXAMPLE

The coloured bars in Fig. 2 show the range of $1/\delta_\nu$ to be tested experimentally for two different cases. The lower end of the intervals represents the flow condition at the stern, while the upper end of the intervals corresponds to x_0. The coloured intervals are found solving Eq. 14 and using Granville's approach to obtain the distributions of c_f. The dark grey bar on the top figure corresponds to a 220-m-long flat plate at 14.5 knots. This is, for instance, at the lower end of the operational speed range for LNG carriers, which typically operate between a cruising speeds range of 13 to 19 knots. The solid line is drawn with Eq. 12 using a coating with $R_a = 8.1$ μm, leading to $k_s = 4.9$ μm. The light grey bar on the bottom figure corresponds to a 3.048-m-long flat plate with a speed of 3.9 knots and it can be representative of a small sailing craft or of a model scale ship hull. The solid line is drawn with a relatively smooth representative coating with $R_a = 3.2$ μm, resulting in $k_s = 1.95$ μm.

3.3 EXPERIMENTAL MEASUREMENTS

3.3.1 MATCHING OF THE FULL SCALE FLOW CONDITIONS

As anticipated above, the friction Reynolds number (R_a/δ_ν) can be replicated in a laboratory using an un-scaled sample of the rough surface. This is possible because the full-scale δ_ν can be replicated in a laboratory. In fact, δ_ν increases slowly with the geometrical length scale (x), but it decreases quickly with the flow velocity. Using, for instance, the $1/7^{th}$ power law (Eq. 16), it can be shown that $\delta_\nu \propto x^{1/14}$ and $\delta_\nu \propto U^{-13/14}$. Hence, the same δ_ν of a large surface occurs on a much smaller surface at a slightly lower velocity. For example, the δ_ν developed over a flat plate at a distance $x_1 = 220$ m from the leading edge at a flow velocity $U_1 = 7.5$ ms^{-1}, is the same as that over a flat plate at a distance $x_2 = 0.025$ m at a flow velocity $U_2 = U_1[(x_2/x_1)]^{1/13} = 3.7$ ms^{-1}. It can also be verified using, for instance, Colebrook's equation for the Darcy friction factor [31], that the same δ_ν occurs at the same flow speed in a fully developed channel flow with a hydraulic diameter of approximately 0.1 m.

With reference to the same example as in Sec. 3.2.5, using the $1/7^{th}$ power law (Eq. 16), we find that $\delta_\nu = 6.9$ μm at the trailing edge of a 220-m-long flat plate travelling at 14.5 knots (7.5 ms^{-1}). We showed that the same δ_ν occurs in a channel with a hydraulic diameter of 0.1 m and a bulk velocity of 3.7 ms^{-1}. However, at the leading edge of the plate, $\delta_\nu = 0$ and it grows up to 6.9 μm over the length of the plate. To achieve a lower δ_ν in a fully-developed channel flow, the flow velocity must be increased. Hence, the maximum attainable flow velocity in the facility determines the minimum δ_ν that can be tested. Fortunately, because $\delta_\nu \propto x^{1/14}$, δ_ν grows very quickly near the leading edge, while it grows slowly after a short distance. Hence, the region near the leading edge of the flat plate, where δ_ν is too small to be measured, is relatively small.

In Sec. 3.2, we showed how to compute the coordinate x_0 such that the frictional resistance of the flat plate from $x = x_0$ to $x = L$ is 99% of the total frictional resistance. We recommended that the minimum δ_ν tested in the fully-developed channel flow is the δ_ν that occurs at a distance x_0 from the leading edge of the plate. For the 220-m-long flat plate, $x_0 = 1.3$ m, where δ_ν is 4.8 μm. This shows that the region where δ_ν is not precisely matched is, indeed, very small compared to the length of the ship; while the range of δ_ν that has to be tested is relatively small.

3.3.2 RECOMMENDED EXPERIMENTAL SETUP

ΔU^+ has to be determined experimentally within the selected range of $1/\delta_\nu$. Both the smooth and the rough surfaces must be tested. These tests have been performed in cavitation tunnels, for instance measuring the forces on a floating element at the wall [6], or velocity profiles and Reynolds stresses using laser Doppler velocimetry [4, 42]. However, a more accurate means to measure ΔU^+ is through the measure of the streamwise pressure gradient and the flow rate in a fully-developed channel flow facility [23, 43]. In fact, indirect methods for the determination of frictional resistance from velocity measurements are highly sensible to scatter in the data [44]. Small misalignment of the floating element can overestimate forces by one order of magnitude [45].

The measure of the pressure gradient allows to compute δ_ν, while the measure of the flow rate allows to compute ΔU^+. The streamwise pressure drop Δp measured between the inlet and the outlet of the test section of a fully-developed channel flow facility is directly correlated to the mean skin friction at the walls, $\overline{\tau}_w$, and thus to δ_ν. Hence, known the δ_ν that has to be achieved, it can be computed the Δp that should be measured to assure that the flow conditions are those desired.

Typical facilities designed for these types of measurements have a high aspect ratio rectangular section where samples of rough surfaces are used for the two large side walls of the channel. To briefly illustrate the principles, let consider a channel with cross sectional area $A_\perp$ and total area of the side walls $A_\parallel$. The difference Δp between the upstream and downstream cross sections, must be balanced by the wall friction $\bar{\tau}_w$ on the side walls, *i.e.* $\Delta p A_\perp = \tau_w A_\shortparallel$. Therefore, in order to achieve the desired δ_ν, the pressure drop must be set to

$$\Delta p = \frac{A_\shortparallel}{A_\perp}\tau_w = \frac{A_\shortparallel}{A_\perp}\frac{\rho\nu^2}{\delta_\nu^2}. \tag{23}$$

Testing a rough and a smooth surface at the same $\bar{\delta}_\nu$, ΔU^+ can be computed from the measurement of the flow rate in the channel for a rough and a smooth surface (Q_r and Q_s, respectively). In fact, knowing the two flow velocities averaged over the cross section ($\bar{U}_r = Q_r/A_\perp$ and $\bar{U}_s = Q_s/A_\perp$), the roughness function can be computed as

$$\Delta U^+ = \frac{\delta_\nu}{\nu}(\bar{U}_s - \bar{U}_r). \tag{24}$$

3.4 FITTING OF THE ROUGHNESS FUNCTION

To illustrate the proposed methodology with an example, we use four realistic data points representative of two antifouling coatings tested in a fully-developed channel flow facility at two different flow speeds each. These values are not exact measurements but realistic values taken from a proprietary database of AkzoNobel's antifouling coatings. This data should only be used as an example of the proposed methodology and to demonstrate the relative differences between methods. The four data points are shown with solid circles in Fig. 2 and is summarised in Table 1.

A roughness function of the type

$$\Delta U^+ = A \ln\left(B + \frac{\lambda}{\delta_\nu}\right) \tag{25}$$

can be used to fit the experimental measured ΔU^+ (dotted line in Fig. 2). A and B are dimensionless parameter while λ is a length in metres.

The parameter λ is not directly related to the roughness geometry but it is an hydrodynamic length scale that depends on the frictional properties of the surface. This approach was originally proposed by Grigson [22], who described ΔU^+ with geometrical series that can be used also when the curve

Table 1: Sample values of two realistic antifouling coatings tested in a fully-developed channel flow facility.

R_a	$1/\delta_\nu$	ΔU^+	A	B	λ
[μm]	[m^{-1}]	[-]	[-]	[-]	[μm]
3.2	5.5×10^4	0.37	1/0.41	1.15	0.28
3.2	8.5×10^4	0.39	1/0.41	1.15	0.28
8.1	1.2×10^5	0.88	1/0.41	1.41	0.21
8.1	2.0×10^5	0.91	1/0.41	1.41	0.21

ΔU^+ vs. $^1/_{\delta_\nu}$ has multiple inflection points. This hydrodynamic length scale λ could be called equivalent sand grain roughness height. However, this has generated some confusion in industry, where the use of the sand grain roughness height is intended as the use of *a priori* correlations such as, for instance, Eq. 12 together with Eq. 13. Moreover, in the proposed approach, the roughness function does not depend only on λ but also on A and B. For this reason, in this paper we do not name λ as equivalent sand grain roughness height. Moreover, we use a dimensional length to highlight that λ cannot be scaled arbitrarily because it is correlated to the specific un-scalable roughness topology.

If more than three conditions are tested, the parameters A, B and λ can be identified by the least square method. On the other hand, if only two conditions are tested, one of these three parameters can be fixed *a priori* and the other two can be computed analytically. If $B = 1$ then in the limit $\delta_\nu \to \infty$, $\Delta U^+ = 0$ as on a smooth surface. Conversely, if we chose $A = {}^1/_\kappa$, then in the limit of $^1/_{\delta_\nu} \to \infty$, ΔU^+ increases with the same slope as Eq. 12, as it should do in fully rough conditions. This latter choice of the parameters was made to draw Eq. 25 in Fig. 2 (dashed lines). In this case, using the subscripts $_L$ and $_U$ for the lower and upper values, respectively, B and λ can be computed with

$$\lambda = \frac{e^{\kappa \Delta U_L^+} - e^{\kappa \Delta U_U^+}}{\frac{1}{\delta_{\nu_L}} - \frac{1}{\delta_{\nu_U}}} \tag{26}$$

and

$$B = e^{\kappa \Delta U_L^+} - \frac{\lambda}{\delta_{\nu_U}}. \tag{27}$$

Table 1 shows the values of the fitting parameters B and λ for the example data in Fig. 2 (dotted lines), where $A = {}^1/_\kappa$.

3.5 WALL FUNCTIONS

Equation 25 can be embedded in a wall treatment for the CFD simulations. The parameters A, B and λ, derived from the experimental measurements, are used as input to characterise a specific coating roughness. Wall functions are used to impose boundary conditions on turbulent quantities for the cells adjacent to the wall and to compute the stress at the wall, τ_w. The first grid point (P) must be at a distance from the wall (y_P) where production and dissipation of turbulent stresses are in equilibrium, and viscous stresses are negligible. Therefore, $y_P \gg \delta_\nu$.

As an example, we coded the wall functions developed by Kim [46] in OpenFOAM v2.4 for the $K-\epsilon$ turbulence model. The $K-\omega$ SST turbulence model is probably more popular in ship hydrodynamics [47], but it works better without wall functions where the boundary layer is fully resolved with a first grid point at $y^+ < 1$. Since the roughness can be modelled only using wall functions, we prefer the $K-\epsilon$ turbulence model. This wall function implementation is based on that by Launder & Spalding [48] for equilibrium boundary layers, and it is extended to account for non constant shear stresses and non-zero pressure gradients. In fact, pressure gradients induce a variation of the shear stress τ from the wall up to (and within) the overlap layer. A modified logarithmic velocity profile and a turbulent kinetic energy K budget, which includes pressure gradients effects, are derived in Kim & Sung-Eun [46]. Only final results relevant to the wall function are reported hereby.

The transport equation for the momentum balance equation, modified for near wall cells in such a way that τ_w satisfies the modified overlap logarithmic law of the wall, is

$$\frac{\widetilde{U_P}}{(\tau_w/\rho)} C_\mu^{1/4} K_P^{1/2} = \frac{1}{\kappa} \ln\left(E y_P \frac{C_\mu^{1/4} K_P^{1/2}}{\nu} \right) - \Delta U^+, \tag{28}$$

where $C_\mu = 0.09$, $E = 8.09$ and K_P is turbulent kinetic energy evaluated at the grid point P. The quantity $\widetilde{U_P}$ is obtained from the streamwise velocity U_P using

$$\widetilde{U_P} = U_P + \\ - \frac{1}{2}\frac{dp}{dx}\left[\frac{y_\nu}{\rho\kappa C_\mu^{1/4} K_P^{1/2}} \ln\frac{y}{y_\nu} + \frac{y_P - y_\nu}{\rho\kappa C_\mu^{1/4} K_P^{1/2}} + \frac{y_P^2}{\rho\nu} \right], \tag{29}$$

where y_ν is the height of the viscous sub-layer computed as

$$y_\nu = 11 \frac{\nu}{C_\mu^{1/4} K_P^{1/2}}. \tag{30}$$

The velocity $\widetilde{U_P}$ modified for the effect of a pressure gradient $^{dp}/_{dx}$ is the main difference from the formulation of Launder & Spalding [48]. When $^{dp}/_{dx} \to 0$, Eq. 28 tends to Eq. 9, *i.e.* $\widetilde{U_P} = U_P$ and the constant stress behaviour is recovered. This can be verified substituting $\tau_w = \rho C_\mu^{1/2} K_P$, which is valid for equilibrium boundary layers, into Eq. 28 for a zero pressure gradient.

The roughness function ΔU^+ in Eq. 28 is found using Eq. 25, where the constants A, B, λ are given as input parameters to the wall function. The viscous length scale

$$\delta_\nu^* = \frac{\nu}{C_\mu^{1/4} K_P^{1/2}}. \tag{31}$$

is used instead of δ_ν [48].

In OpenFOAM 2.4, τ_w is applied using a boundary condition on the turbulent kinetic energy, such that

$$\nu_t = \frac{\tau_w}{\rho}\frac{y_P}{U_P} - \nu. \tag{32}$$

The above expression can be derived from the diffusive term of the Reynolds-averaged Navier-Stokes (RANS) equation, where only the wall normal gradient of velocity is considered

and approximated by U_P/y_P. At the beginning of each iteration, a new value of τ_w is computed from Eq. 28 starting from previous values of U_P, K_P, and $^{dp}/_{dx}$; and the new τ_w is substituted into Eq. 32. Once the value of ν_t has been determined and used as a boundary condition for near wall cells, the RANS equation for the averaged velocity U and pressure p can be solved.

The new values of velocity are then used to solve the transport equation for K. At the wall, a zero gradient boundary condition $^{dK}/_{dy} = 0$ is applied and the transport equation for K is modified adding an additional production $\overline{P}_K$ term and dissipation $\bar{\epsilon}$ term. For quadrilateral cells, these are defined by the depth averages over the height y_n of the cell as

$$\overline{P}_K = \frac{1}{y_n}\int_0^{y_n} \tau_t \frac{\partial U}{\partial y} dy, \qquad \bar{\epsilon} = \frac{1}{y_n}\int_0^{y_n} \epsilon dy. \tag{33}$$

According to the two-layer approach of Kim [46], the cell adjacent to the wall is split in a viscous sub-layer that ranges from the wall up to y_ν and where inertia could be neglected, and a fully turbulent zone for $y > y_\nu$. Thus, the turbulent quantities in Eq. 33 vary within the height of the cell as

$$\begin{aligned} \tau_t = & \begin{cases} 0 & \text{for } y < y_\nu, \\ \tau_w + \frac{1}{2}\frac{dp}{dx}(y_\nu + y) & \text{for } y > y_\nu; \end{cases} \\ \epsilon = & \begin{cases} 2\nu K_P y_\nu^{-2} & \text{for } y < y_\nu, \\ \frac{K_P^{3/2} C_\mu^{3/4}}{\kappa y} & \text{for } y > y_\nu. \end{cases} \end{aligned} \tag{34}$$

Expressions of $\overline{P}_K$ and $\bar{\epsilon}$ resulting from the integrals in Eq. 33 with Eq. 34 are "hard coded" in the wall function, providing an explicit way to compute production and dissipation source terms in the K-equation from previous values of K_P, τ_w, y_ν and $^{dp}/_{dx}$.

Finally, the ϵ transport equation is not solved for near-wall cells. Instead, the value of ϵ at the centroid P is set according to Eq. 34, and reads

$$\epsilon_P = \frac{K_P^{3/2} C_\mu^{3/4}}{\kappa y_P}. \tag{35}$$

4 CASE STUDY

As an example, we consider a parabolic Wigley hull, whose geometry is defined by

$$y = \frac{W}{2}\left[1 - \left(\frac{2x - L}{L}\right)^2\right]\left[1 - \left(\frac{2z}{T}\right)^2\right], \tag{36}$$

where W, L, T are beam, length and draft, respectively. Their ratios are such that $L : W : T = 10 : 1 : 0.625$.

Two case studies are considered, where the lengths and speeds are the same as those used in the example in Sec. 3.2.5, and the antifouling coating products are the same as those presented in Sec. 3.4, Table 1. In particular, we consider the relatively smooth surface with $R_a = 3.2$ μm for the 3.048-m-long hull sailing at 3.9 knots ($Re = 4.5 \times 10^6$), and the rougher surface with $R_a = 8.1$ μm for the 220-m-long hull sailing at 14.5 knots ($Re = 1.2 \times 10^9$). These two case studies are denoted as low-Re and highRe case study, respectively.

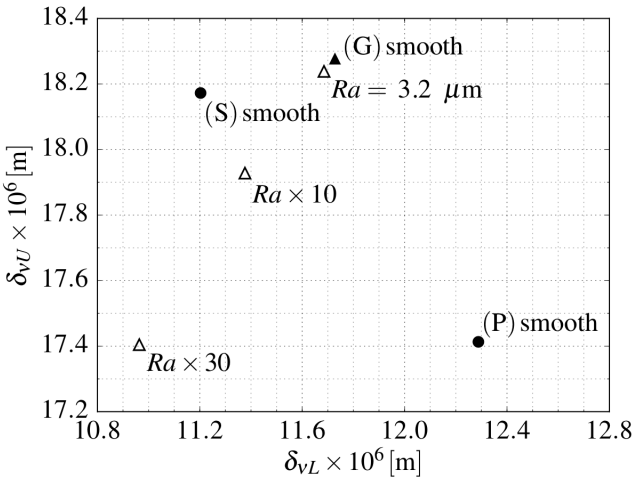

Figure 3: Lower and upper bounds of the viscous length range to account for 99% of overall skin friction, computed with (P), (S), (G) for a smooth surface, and (G) with different average roughness heights (low-Re case).

4.1 PREDICTED FLOW CONDITIONS

Figure 3 shows the lower (δ_{ν_L}) and upper (δ_{ν_U}) bounds for the low-Re case study. These are computed with the correlation lines (P), (S), and (G) for a smooth surface, and (G) for a roughness $R_a = 3.2$ μm. Two other cases computed with (G) and higher roughness heights are reported for comparison. Taking (G) in smooth condition as a baseline, the differences for the computed lower bounds of (P), (S), and (G) with the smallest roughness height ($R_a = 3.2$ μm) are $+4.8\%$, -4.5% and -0.4%, respectively. For the upper bounds, we find -4.7%, -0.6% and -0.2%, respectively.

When a higher roughness height is considered, we observe a reduction in the values of both δ_{ν_L} and δ_{ν_U} compared to the smooth conditions. This is due to the higher shear stress at the wall. The lower bounds δ_{ν_L} for the cases with $R_a = 32$ μm and $R_a = 96$ μm are 3.0% and 6.5% lower than the baseline, respectively.

In this low-Re test case, considering low roughness heights gives hardly appreciable differences compared to a smooth case. However, this does not mean that when the specific rough surface is tested in the fully-developed channel flow facility, it should be expected to measure small ΔU^+. In fact, the estimate of ΔU^+ is based on the value of R_a through Eq. 12 with Eq 13, which might not give reasonable results for all the variety of roughness types.

The lower and upper bounds for the viscous length are computed with the friction line (G) for rough surfaces. For the low- and high-Re model, δ_ν ranges from 11.7 μm and 18.2 μm, and from 4.96 μm and 6.91 μm, respectively. The minimum δ_ν occurs at $^{x_0}/_L = 0.006$ for both models.

4.2 NUMERICAL SIMULATIONS

The RANS equations for Newtonian fluids and steady, incompressible flow are solved with the finite-volume CFD code OpenFOAM v2.4. A $K - \epsilon$ turbulence model is used for the computation of turbulent viscosity. Limited central dif-

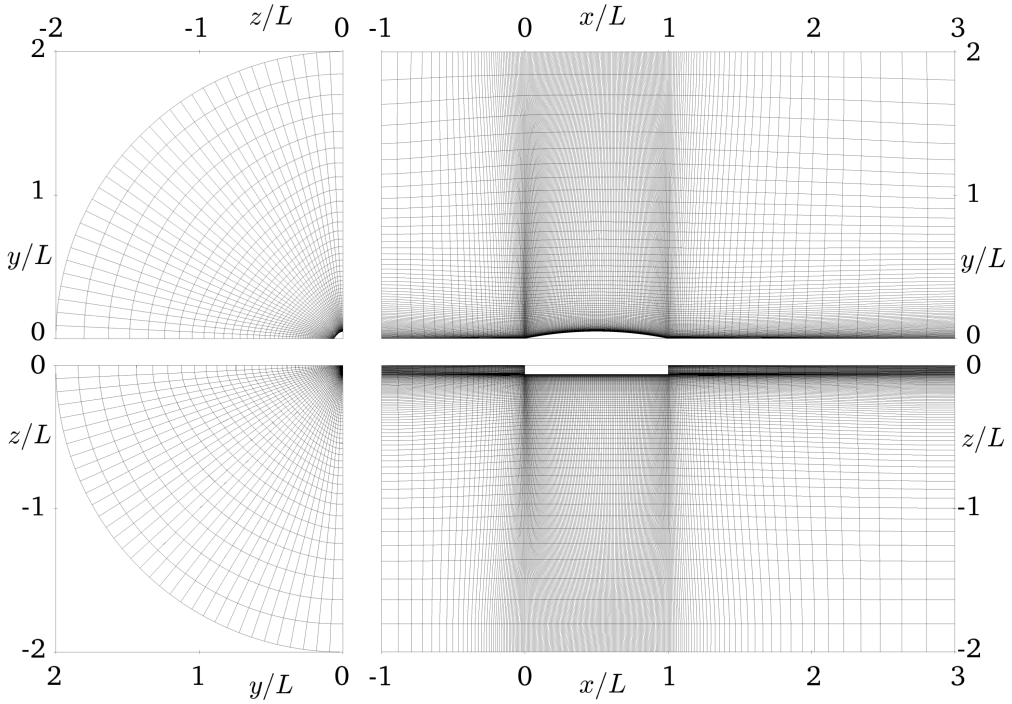

Figure 4: Discretised computational domain. The water plane is shown on the upper right and the hull centerline plane is shown on the lower right of the figure. Cross sections at midship and at stern are shown on the upper left and lower left of the figure, respectively.

ferencing schemes are used for the discretisation of gradients (*cellLimited Gauss linear* 1) and Laplacian terms (*Gauss linear limited* 0.33) in all transport equations. A bounded central differencing scheme with limiters (*bounded Gauss limitedLinear* 1) and a bounded second order upwind (*bounded Gauss linearUpwindV*) are used for the divergence terms in the convective transport of turbulent quantities and velocity, respectively. Steady state solutions were achieved using the SIMPLE scheme for the pressure-velocity coupling.

The free surface boundary is neglected, instead, a symmetry condition is imposed at the water plane ($z = 0$). Only half of the hull is considered, using a symmetry condition on the symmetry plane ($y = 0$). The velocity inlet boundary is at one hull's length upstream from the bow ($x = -L$) and the pressure outlet is at two lengths downstream from the stern ($x = 3L$). A velocity inlet boundary condition is also used for the far field plane, a lateral cylindrical surface at two lengths cross stream ($y^2 + z^2 = 4L^2$). For the hull's surface, a zero velocity and null normal gradient of pressure is imposed and boundary conditions for turbulent quantities are provided by wall functions.

A single-block H-O structured mesh is used to discretise the computational domain. The number of grid points in the longitudinal, radial and tangential directions are $(253, 89, 44)$ for the low-Re model, and $(693, 89, 55)$ for the high-Re model, totalling 0.95 and 3.3 million cells, respectively. Figure 4 shows the computational domain used for the simulations of the low-Re model. Average spacings on the hull's surface are $\Delta x/L = 0.007$ and $\Delta z/L = 0.0015$ for the low-Re model, and $\Delta x/L = 0.0025$ and $\Delta z/L = 0.0018$ for the high-Re model. For both models, refinements near the bow, keel and stern are applied. In the wall normal direction, a constant spacing along the hull is used, leading to a variable y^+ in the range $[21 - 96]$ for the low-Re model and y^+ in the range $[32 - 199]$ for the high-Re one.

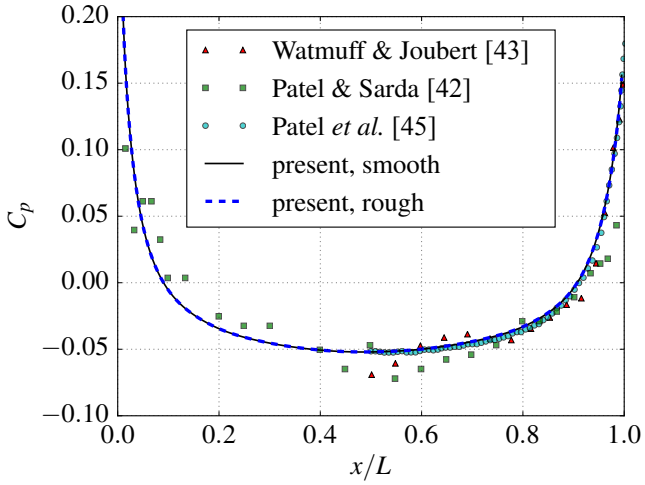

Figure 5: Pressure coefficient distribution C_p computed along the waterline and comparison with wind tunnel experiments on double hull models for the low-Re model.

4.3 PRESSURE DISTRIBUTION

In order to test the proposed wall functions, steady state RANS simulations at zero Froude number (flat water surface) are performed. Both smooth and rough conditions are modelled. For the smooth case, ΔU^+ is set to 0 in Eq. 32. For the rough surface, Eq. 25 is substituted in Eq. 32.

For the low-Re model, the pressure and friction coefficient along the hull can be compared with experimental data of Patel & Sarda [49] and Watmuff & Joubert [50]. Experi-

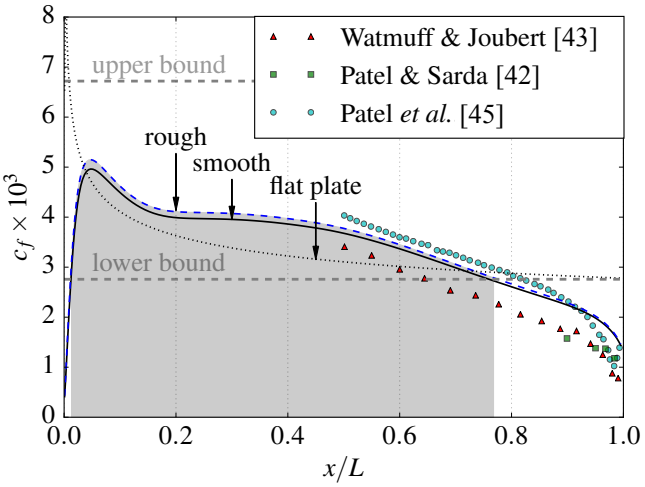

Figure 6: Friction coefficient c_f computed along the waterline and comparison with wind tunnel experiments on double hull models for the low-Re model. The region where the values of ΔU^+ are measured, *i.e.* non extrapolated, is highlighted in grey.

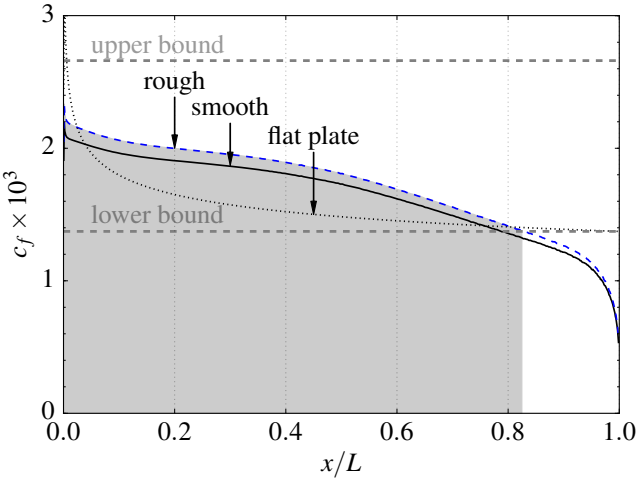

Figure 7: Friction coefficient c_f computed along the waterline for the high-Re model. The region where the values of ΔU^+ are measured, *i.e.* non extrapolated, is highlighted in grey.

ments were performed in a closed-loop wind tunnel with a low freestream turbulence level on a 3.048-m-long double model. In the study of Patel & Sarda [49], the pressure distribution was measured by surface pressure taps, and average velocities were measured with a five-hole pitot tube. The Clauser method [51] was used by Patel *et al.* [52] to compute the friction coefficient from measurements of the velocity profiles.

Figure 5 shows a numerical-experimental comparison on the pressure coefficient C_p along the hull at the water plane. CFD results are in good agreement with the experimental data, although a high scatter is observed in the measurements. Near the stern, the computed C_p agrees particularly well with the measurements of Watmuff & Joubert [50]. Although the two experiments were run under similar conditions [52], a possible cause of disagreement could be the slightly thicker sections near the bow and the stern used by Patel & Sarda [49] than the one used by Watmuff & Joubert [50], which is the same used in the present simulations. Numerical data from the RANS simulation of Patel *et al.* [52] are also reported in Fig. 5, showing an excellent agreement with the present computation. The smooth and rough distributions of C_p in Fig. 5 are virtually indistinguishable, and the same is true also for the high-Re model (figure not included for brevity).

4.4 FRICTION STRESS DISTRIBUTION

Figure 6 shows the friction coefficient at the same locations as Fig. 5. The present results for the smooth surface are higher than the experimental data, but lower than the RANS simulations of Patel *et al.* [52]. The differences between the numerical and experimental data require further investigation. However, the absolute differences of τ_w that were measured experimentally in the wind tunnel are as small as ca. 0.1 Pa.

The frictional resistance for a flat plate computed with the friction line (G) rough is also presented for comparison together with the predicted lower and upper bounds of c_f to account for 99% of the overall skin friction. Towards the leading edge, because the correlation line neglects the presence of the stagnation point, $c_f \to \infty$, $1/\delta_\nu \to \infty$ and $\Delta U^+ \to \infty$. Conversely, the bow is a stagnation point and thus $c_f = 0$, $1/\delta_\nu = 0$ and $\Delta U^+ = 0$. The effect of the stagnation point is limited to a narrow region near the bow, where the maximum c_f that was cautiously estimated in Sec. 4.1 results in being higher than the maximum c_f effectively computed on the hull. In fact, inevitably, there is a region very near the bow where c_f is even lower than the estimated one. However, the low c_f is associated with low $1/\delta_\nu$ and low ΔU^+ and, hence, it is expected that the effect of the roughness would be negligible. For a more accurate estimate, the lower bound of the experimental range can be decreased. The limiting factor at the lower end of the $1/\delta_\nu$ range, is the available accuracy in the measurement of small flow rates and small pressure drops along the channel.

From midship up to 85% of the hull length, c_f decreases almost linearly due to the convex shape of the hull and the resulting thickening of the boundary layer. The slope of c_f varies only slightly from the region with almost zero pressure gradient ($x/L \in [0.4 - 0.6]$, cf. Fig. 5) to the region where a mild adverse pressure gradient exists ($x/L \in [0.6 - 0.85]$). Conversely, near the stern, the steep pressure recovery induces a significant decrease of τ_w and $1/\delta_\nu$. The stern of the Wigley hull is also a stagnation point, where c_f, τ_w and $1/\delta_\nu$ vanish. This would not be the case on hulls with immersed transoms, where the flow velocity at the stern is not zero.

The grey band in Fig. 6 shows the region where the values of ΔU^+ used in the wall function were measured experimentally and not extrapolated. In this region, $1/\delta_\nu$ at full scale is within the range tested at model scale. A similar result is shown in Fig. 7 for $Re = 1.2 \times 10^9$. The overall frictional resistance for the rough case is found to be 2.8% and 4.6% higher than the smooth case for the low- and high-Re, respectively. These figures are consistent with the increased influence of roughness expected for the high-Re model, for which a surface with higher ΔU^+ values and an higher velocity than the low-Re model have been used. The part of the hull within the grey region in Figs. 6 and 7 accounts for 88% and 90%, respectively, of the total friction difference between the smooth

and rough hulls at the two Re.

The upper bound is never reached, showing that the maximum flow rate that must be achieved experimentally is, in fact, limited. On the other hand, the flow velocity near the stern varies significantly between different hulls. For low speed displacement hulls, such as the Wigley hull, a significant thickening of the boundary layer should be expected, and thus the lower bound could be decreased. Conversely, for hulls with immersed transoms, the lower bound computed as in the proposed methodology should be acceptable.

It is important to note that the use of the proposed wall functions prevents scaling the results based on Re only. The computed friction *coefficient* is valid only for the considered Re and L. For example, if the geometry was scaled and the velocity of the water adjusted to achieve the same Re, a different δ_ν would be computed, resulting in a different ΔU^+ and friction coefficient. The wind tunnel experiments presented in Fig. 6 are performed at the same Re and L as those modelled numerically, and thus the same friction coefficient should be found. The experiments are performed in air at 15 times higher flow speed than in the simulations.

4.5 COMPARISON WITH OTHER PROCEDURES

In this section the proposed approach is compared with two alternative procedures that could be used to estimate the effect of a rough surface on the computed frictional resistance of a full scale ship. The previously considered high-Re model, where the hull is coated with a representative antifouling coating products with $R_a = 8.1$ μm, is used of this comparison.

As a first alternative procedure, the roughness effects could be introduced into the wall function simply measuring the roughness geometry of the surface and then using Eq. 13 to find the equivalent sand grain roughness height k_s. With this procedure, no hydrodynamic measurement is performed and the roughness function is only function of k_s ($\Delta U^+ = \Delta U^+(k_s)$). A wall function formulation based on Colebrook's Eq. 12 could be used into the CFD model. However, standard wall functions provided in many commercial CFD softwares (*e.g.* FLUENT, CFX, STAR-CCM+) are usually based on Nikuradse's work [27], thus, new coding is required in order to adopt the different formulation. As described by Demirel *et al.* [20] the input can be modified *ad hoc* to force the standard formulations into a Colebrook's type behaviour, without new coding involved.

A second alternative approach is to measure the frictional performance of the coated surface (*e.g.* in a fully-developed channel flow facility), and to use a roughness function of the type in Eq. 25 to fit the experimental data. Fixing $A = 1/\kappa$ and $B = 1$ gives the possibility of using a standard wall function formulation, similarly to the previous approach, based on Colebrook's roughness function. In other terms, Eq. 12 is equivalent to Eq. 25 with $A = 1/\kappa$, $B = 1$ and taking λ as equivalent to $0.26k_s$. Hence, the roughness function will be a function of only one free parameter, λ, which is estimated during the fitting ($\Delta U^+ = \Delta U^+(\lambda)$).

These alternative procedures are compared in Fig. 8 together with the present method, where the roughness function

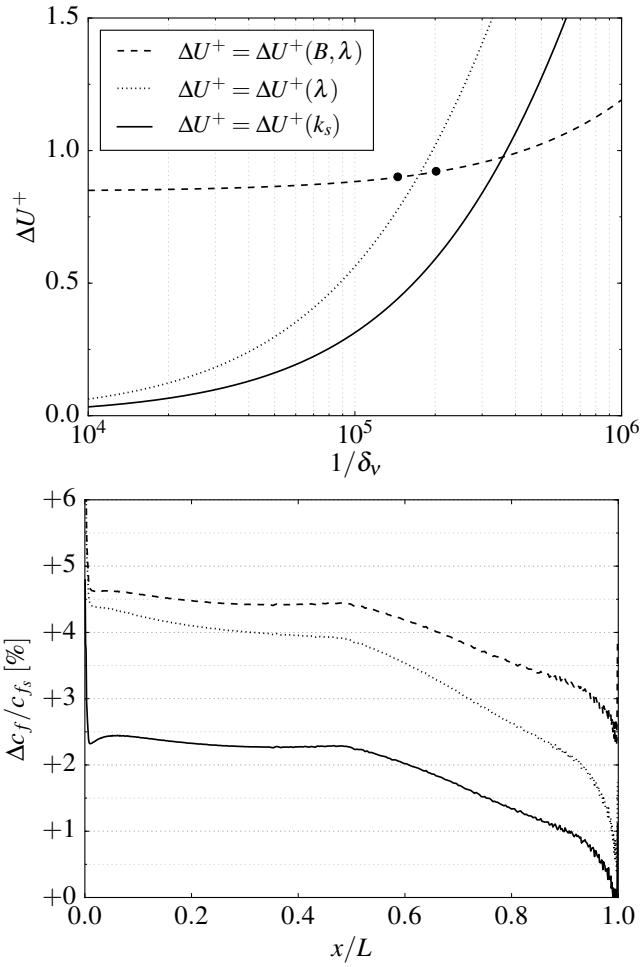

Figure 8: Variation Δc_f between smooth and rough friction coefficient distributions computed using different roughness functions ΔU^+, expressed a percentage of the smooth c_{f_s}. Distributions at waterline (bottom) are computed for the high-Re CFD model using the respective ΔU^+ (top). Circles represent experimental measured ΔU^+ for a coated surface with $R_a = 8.1$ μm. Least square fitting of Eq. 25 (fixed $A = 1/\kappa$) results in $B = 1.41$, $\lambda = 0.21$ μm for the dashed line and $B = 1$, $\lambda = 2.59$ μm for the dotted line. Solid line corresponds to Eq. 12 with $k_s = 0.61R_a = 4.9$ μm.

depends on two free parameters, B and λ, that are estimated fitting Eq. 25 to the experimental data ($\Delta U^+ = \Delta U^+(B,\lambda)$). At the top of Fig. 8 the roughness functions for the three different procedures are shown together with the experimental data. The dotted and dashed lines represent the least square fitting of the experiments using Eq. 25 with one and two free parameters, $\Delta U^+ = \Delta U^+(\lambda)$ and $\Delta U^+ = \Delta U^+(B,\lambda)$, respectively. For the solid line ($\Delta U^+ = \Delta U^+(k_s)$), no fitting is involved, as the only parameter in Eq. 12 is found from R_a and Eq. 13.

Each ΔU^+ is then used in Eq. 28, for the definition of U_P in the wall function formulation, and the correspondent rough friction coefficient distribution (c_{f_r}) is computed for the high-Re CFD model. In Fig. 8 (bottom) the variation $\Delta c_f/c_{f_s}$ for each procedure is plotted along the hull at the waterline, where $\Delta c_f = c_{f_r} - c_{f_s}$ is the difference between the rough (r) and a smooth (s) distribution. Importantly, we observe that the k_s-based method ($\Delta U^+ = \Delta U^+(k_s)$) under-

estimates the c_f-penalty (computed as c_f rough over smooth) by more than 2% when compared to the present approach ($\Delta U^+ = \Delta U^+(B, \lambda)$). In other terms, the c_f distribution computed with the former roughness function is shifted below the one computed with the latter by 2%, with respect to the smooth c_{f_s}. However, because no experimental testing is involved within the k_s-approach, this difference highly depends on how well the used correlation between the geometry and k_s suits the specific rough surface studied. When the $\Delta U^+ = \Delta U^+(\lambda)$ approach is considered (dotted line), differences with the present method falls around 0.5%.

5 CONCLUSIONS

The presented paper can be used as a practical guideline for assessing the effect of different fouling control coatings on the hull's frictional resistance in different sailing conditions. The proposed methodology foresees experiments in a fully-developed channel flow facility and CFD simulations, where wall functions are informed by the best fit of the experimental data of two parameters (B and λ).

The methodology is based on the observation that there is no universal formulation that allows estimating the frictional resistance due to a rough surface based on its geometry and the flow conditions. Therefore, measurements must be performed for every surface and flow condition. Moreover, the roughness geometry depends on the material, the manufacturing process, the finishing, *e.t.c.*. Therefore, it is proposed that an un-scaled sample of the surface is tested in a fully-developed channel flow facility.

Different methods to estimate the experimental flow conditions to be tested are discussed. The tests can be performed at lower Reynolds numbers than at full scale, as long as the full-scale roughness Reynolds number is matched. The frictional resistance due to the roughness (in the form of the friction function ΔU^+) can be measured from the difference in flow rate between the tests of a smooth and a rough surface. An equation for the fit of the experimental data is proposed, and the parameters of this equation are used as input for a wall function. The wall function for the turbulence model $K-\epsilon$, as implemented in OpenFOAM, is presented. The adaptation of the proposed wall function to other turbulent viscosity models and similar CFD codes should be straight forward.

Examples of the proposed methodology are presented for two case studies, where the proposed wall function is tested for a Wigley hull at Reynolds numbers of 4.5×10^6 and 1.2×10^9, respectively. For the smooth case, a good agreement is observed with previous experimental and numerical data, although the data in literature present a high scatter. It is shown that the proposed methodology can enable higher accuracy than other similar approaches when the surface does not follow established correlations between the surface roughness and the equivalent sand grain roughness.

6 ACKNOWLEDGEMENT

This work has been funded by AkzoNobel's Marine and Protective Coatings business (International Paint Ltd.). AkzoNobel is grateful to Prof. Mehmet Atlar (formerly at Newcastle University and now at Strathclyde University, UK), Mr George Politis and Miss Irma Yeginbayeva for having contributed to establish the database of antifouling coating product performances, from which realistic values have been used in this paper.

7 Appendix

The numerical uncertainty on the computation of the frictional resistance is quantified using the method described by Viola *et al.* [53]. Only the uncertainty due to the grid discretisation is considered as it is regarded to be the most significant source of uncertainty. Simulations are dubbed as converged when the residuals of the pressure drop by at least 4 orders of magnitude from their initial value, and the value of total frictional resistance (R_L) change by less than 0.01 in the last two iterations%.

Starting from the low- and high-Re reference models described in Sec. 4.2 (here addressed with the subscript "ref"), two sets of grids are generated refining and coarsening the grid uniformly in all three directions. Each i-mesh is obtained applying a factor $r_i = \Delta_i/\Delta_{\text{ref}}$ to the average spacing Δ of grid nodes but keeping constant their distribution on the edges of the computational domain. Although desirable, perfect geometrical similarity between the meshes is difficult to obtain because grid nodes are each time projected onto the hull surface.

Table 2 and 3 summarise the total number of cells (N_c) and number of grid nodes in the streamwise (N_x), normal (N_y), and girthwise (N_z) directions. For each set of grids, the values of normalised resistance $\phi_i = R_{L_i}/R_{L_{\text{ref}}}$ are fitted into Eq. 37 with c, ϕ_0, p as free parameters.

$$\phi_i = c r_i^p + \phi_0 \tag{37}$$

The exponent p is a measure on how the numerical error decreases refining the mesh and its value should be close to the order of accuracy of the numerical scheme adopted. Although second order schemes are adopted in all the simulations, the use of limiting factors and upwind-biased formulations (cf. Sec. 4.2) for stability purposes lowers the theoretical accuracy below 2. In fact, the exponent p found for the low- and high-Re mesh sets is 0.77 and -0.09, respectively.

Following [53], the grid uncertainty U_g is then computed using:

$$U_g = 1.5 \frac{\phi_{\text{max}} - \phi_{\text{min}}}{1 - \frac{r_{\text{min}}}{r_{\text{max}}}} + \sigma, \tag{38}$$

where σ is the standard deviation of the fitting procedure and the subscripts "max" and "min" indicate the maximum and minimum values found within each mesh set. From Eq. 38, the grid uncertainty is estimated to be 0.88% for the low-Re model and 1.59% for the high-Re one.

REFERENCES

[1] A. L. Braslow and E. C. Knox. Simplified method for determination of critical roughness particles for

Table 2: Grid set parameters for the low-Re model.

i	r_i	$N_c \times 10^{-6}$	N_x	N_y	N_z	y^+_{avg}
1	0.63	3.81	400	141	69	41
2	0.79	1.89	317	112	55	53
3	1.00	0.95	253	89	44	67
4	1.26	0.48	201	71	35	86
5	1.59	0.24	160	57	28	108

Table 3: Grid set parameters for the high-Re model.

i	r_i	$N_c \times 10^{-6}$	N_x	N_y	N_z	y^+_{avg}
1	0.50	26.31	1385	177	109	72
2	0.79	6.58	873	112	69	112
3	1.00	3.29	693	89	55	143
4	1.26	1.66	551	71	44	173

boundary-layer transition at Mach numbers from 0 to 5. Report, NACA TN 4363, 1958.

[2] M. P. Schultz. Effects of coating roughness and biofouling on ship resistance and powering. *Biofouling: The Journal of Bioadhesion and Biofilm Research*, 23:5:331–341, 2007.

[3] M. P. Schultz. Frictional resistance of antifouling coating systems. *ASME Journal of Fluids Engineering*, 126:1039–1047, 2004.

[4] M. Candries. *Drag, Boundary-Layer and Roughness Characteristics of Marine Surfaces Coated With Antifoulings.* PhD Thesis, University of Newcastle, 2001.

[5] C. E. Weinell, K. N. Olsen, M. W. Christoffersen, and S. Kiil. Experimental study of drag resistance using a laboratory scale rotary set-up. *Biofouling*, 19(sup1):45–51, 2003.

[6] R. I. Karlsson. The effect of irregular surface roughness on the frictional resistance of ships. In *International Symposium on Ship Viscous Resistance*, 1978. Paper 9.

[7] K. L. Kirkman. The evolving role of the towing tank. In JP Den Hartog, editor, *The Fourth Chesapeake Sailing Yacht Symposium, Annapolis, MD, US*, pages 129–155, 1979.

[8] J. H. Milgram. Fluid mechanics for sailing vessel design. *Annual Review of Fluid Mechanics*, 30(1):613–653, 1998.

[9] L. Larsson. Scientific methods in yacht design. *Annual Review of Fluid Mechanics*, 22(1):349–385, 1990.

[10] G. Hughes. Friction and form resistance in turbulent flow and a proposed formulation for use in model and ship correlation. *Transactions of the Royal Institutions of Naval Architects*, 96:314–376, 1954.

[11] R. L. Townsin. The ITTC line-its genesis and correlation allowance. *The Naval Architect*, pages E359–E362, 1985.

[12] R. L. Townsin. The correlation of added drag with surface roughness parameters. In *Recent Developments in Turbulence Managment*, pages 181–191. Kluwer Academic Publishers, Netherlands, 1991.

[13] A. J. Musker. *Turbulent Shear-Flows Near Irregularly Rough Surfaces With Particular Reference to Ships' Hulls*. PhD Thesis, University of Liverpool, 1977.

[14] L. Larsson, F. Stern, and M. Visonneau, editors. *Numerical Ship Hydrodynamics - An Assessment of the Gothenburg 2010 Workshop*. Springer, 2010.

[15] I. M. Viola, S. Bartesaghi, S. Della Rosa, and S. Cutolo. On the use of CFD for the design of yacht hulls. *Int. J. Small Cr. Technol.*, 155(2):81–93, 2013.

[16] ITTC. Practical guidelines for ship CFD applications. In *Recommended Procedures and Guidelines*. Report 7.5-03-02-03, 2014.

[17] I. M. Viola, R. G. J. Flay, and R. Ponzini. CFD analysis of the hydrodynamic performance of two candidate America's Cup AC33 hulls. *Int. J. Small Cr. Technol.*, 154(1), 2012.

[18] D. C. Wilcox. *Turbulence Modeling for CFD*. DWC Industries, 3rd edition, 2006.

[19] D. Apsley. CFD calculation of turbulent flow with arbitrary wall roughness. *Flow, Turbulence and Combustion*, 78(2):153–175, 2007.

[20] Y. K. Demirel, M. Khorasanchi, O. Turan, A. Incecik, and M. P. Schultz. A CFD model for the frictional resistance prediction of antifouling coatings. *Ocean Engineering*, 89:21–31, 2014.

[21] Yigit Kemal Demirel, Osman Turan, and Atilla Incecik. Predicting the effect of biofouling on ship resistance using CFD. *Applied Ocean Research*, 62:100–118, 2017.

[22] C. W. B. Grigson. Drag losses of new ships caused by hull finish. *Journal of Ship Research*, 36:182–196, 1992.

[23] M. Leer-Andersen and L. Larsson. An experimental/numerical approach for evaluating skin friction on full-scale ships with surface roughness. *Journal of Marine Science and Technology*, 8:26–36, 2003.

[24] M. R. Raupach, R. A. Antonia, and S. Rajagopalan. Rough-wall turbulent boundary layers. *Appl. Mech. Rev.*, 44(1):1–25, 1991.

[25] J. Jimenez. Turbulent flows over rough walls. *Annual Review of Fluid Mechanics*, 36:173–196, 2004.

[26] M. P. Schultz and A. Myers. Comparison of three roughness function determination methods. *Experiments in Fluids*, 35(4):372–379, 2003.

[27] J. Nikuradse. Law of flow in rough pipes. Report, NACA TM, 1933.

[28] H Schlichting. Tragflügeltheorie bei Ueberschallgeschwindigkeit. *ZAMM - Journal of Applied Mathematics and Mechanics / Zeitschrift für Angewandte Mathematik und Mechanik*, 16(6):363–365, 1936.

[29] F. R. Hama. Boundary layer characteristics for smooth and rough surfaces. *Trans. Soc. Naval Archit. Mar. Eng.*, 62:333–358, 1954.

[30] D. I. Pullin, N. Hutchins, and D. Chung. Turbulent flow over a long flat plate with uniform roughness. *Physical Review Fluids*, 2(8), 2017.

[31] C. F. Colebrook. Turbulent flow in pipes, with particular reference to the transition region between the smooth and rough pipe laws. *Journal of ICE*, 11(4):133–156, 1939.

[32] R. L. Simpson. Generalized correlation of roughness density effects on turbulent boundary-layer. *AIAA Journal*, 11(2):242–244, 1973.

[33] Michael P. Schultz. The Relationship Between Frictional Resistance and Roughness for Surfaces Smoothed by Sanding. *Journal of Fluids Engineering*, 124(2):492, 2002.

[34] K.A. Flack and M.P. Schultz. Review of hydraulic roughness scales in the fully rough regime. *ASME Journal of Fluids Engineering*, 132(4), 2010.

[35] Karen A. Flack, Michael P. Schultz, and William B. Rose. The onset of roughness effects in the transitionally rough regime. *International Journal of Heat and Fluid Flow*, 35:160–167, 2012.

[36] U. O. Unal. Correlation of frictional drag and roughness length scale for transitionally and fully rough turbulent boundary layers. *Ocean Engineering*, 107:283–298, 2015.

[37] O Turan, Y K Demirel, S Day, and T Tezdogan. Experimental Determination of Added Hydrodynamic Resistance Caused by Marine Biofouling on Ships. *Transportation Research Procedia*, 14(0):1649–1658, 2016.

[38] F. M. White. *Fluid Mechanics*. McGraw-Hill, 4th edition, 2010.

[39] K. E. Schoenherr. Resistance of flat surfaces moving through a fluid. *Transactions SNAME*, 40:279–313, 1932.

[40] P. S. Granville. Three indirect methods for the drag characterisation of arbitrarily rough surfaces on flat plates. *Journal of Ship Research*, 31(1):70–77, 1987.

[41] D. Coles. The law of the wake in the turbulent boundary layer. *Journal of Fluid Mechanics*, 1(2):191–226, 1956.

[42] M. P. Schultz and G. W. Swain. The effect of biofilms on turbulent boundary layers. *Transactions of the ASME*, 121:44–51, 1999.

[43] K. A. Flack, M. P. Schultz, J. M. Barros, and Y. C. Kim. Skin-friction behavior in the transitionally-rough regime. *International Journal of Heat and Fluid Flow*, 61:21–30, 2016.

[44] J. M. Walker. The application of wall similarity techniques to determine wall shear velocity in smooth and rough wall turbulent boundary layers. *Journal of Fluids Engineering-Transactions of the ASME*, 136(5):10, 2014.

[45] T. J. Hanratty and J. A. Campbell. Measurement of wall shear stress. In R.J. Goldstein, editor, *Fluid Mechanics Measurement (2nd Ed.)*, pages 575–648, Philadelphia, PA, 1996. Taylor & Francis.

[46] Sung-Eun Kim. A near-wall treatment using wall functions sensitized to pressure gradient. In FED-ASME, editor, *Separated and Complex Flows*, volume 217. ASME, 1995.

[47] Lars Larsson, Frederick Stern, and Michel Visonneau. *Numerical ship hydrodynamics: an assessment of the Gothenburg 2010 workshop*. Springer, 2013.

[48] B. E. Launder and D. B. Spalding. The numerical computation of turbulent flows. *Computer Methods in Applied Mechanics and Engineering*, 3(2):269 – 289, 1974.

[49] V. C. Patel and O. P. Sarda. Mean-flow and turbulence measurements in the boundary layer and wake of a ship double model. *Experiments in Fluids*, 8:319–335, 1990.

[50] J. H. Watmuff and P. N. Joubert. Pressure coefficient and skin friction coefficient distributions for the Wigley hull. Report, University of Melbourne, Australia, 1983. Data taken from Patel et al., 1988.

[51] F. H. Clauser. Turbulent boundary layers in adverse pressure gradients. *J. Aerosp. Sci.*, 21:91–108, 1954.

[52] V. C. Patel, H. C. Chen, and S. Ju. Ship stern and wake flows: Solutions of the fully-elliptic Reynolds-Averaged Navier-Stokes Equations and comparisons with experiments. Report, IIHR No. 323, The University of Iowa, 1988.

[53] I. M. Viola, P. Bot, and M. Riotte. On the uncertainty of CFD in sail aerodynamics. *International Journal for Numerical Methods in Fluids*, 72(11):1146–1164, 2013.